Journal of Medicinal Chemistry

pubs.acs.org/jmc

Article

Comparative Study of Sonodynamic and Photoactivated Cancer Therapies with Re(I)-Tricarbonyl Complexes Comprising Phenanthroline Ligands

Rajesh Kushwaha, Virendra Singh, Silda Peters, Ashish Kumar Yadav, Tumpa Sadhukhan,* Biplob Koch,* and Samya Banerjee*

Cite This: *J. Med. Chem.* 2024, 67, 6537−6548

Read Online

ACCESS | Metrics & More | Article Recommendations | Supporting Information

ABSTRACT: Herein, we have compared the effectivity of light-based photoactivated cancer therapy and ultrasound-based sonodynamic therapy with Re(I)-tricarbonyl complexes (**Re1**−**Re3**) against cancer cells. The observed photophysical and TD-DFT calculations indicated the potential of **Re1**−**Re3** to act as good anticancer agents under visible light/ultrasound exposure. **Re1** did not display any dark- or light- or ultrasound-triggered anticancer activity. However, **Re2** and **Re3** displayed concentration-dependent anticancer activity upon light and ultrasound exposure. Interestingly, **Re3** produced $^1O_2$ and OH$^\bullet$ on light/ultrasound exposure. Moreover, **Re3** induced NADH photo-oxidation in PBS and produced H_2O_2. To the best of our knowledge, NADH photo-oxidation has been achieved here with the Re(I) complex for the first time in PBS. Additionally, **Re3** released CO upon light/ultrasound exposure. The cell death mechanism revealed that **Re3** produced an apoptotic cell death response in HeLa cells via ROS generation. Interestingly, **Re3** showed slightly better anticancer activity under light exposure compared to ultrasound exposure.

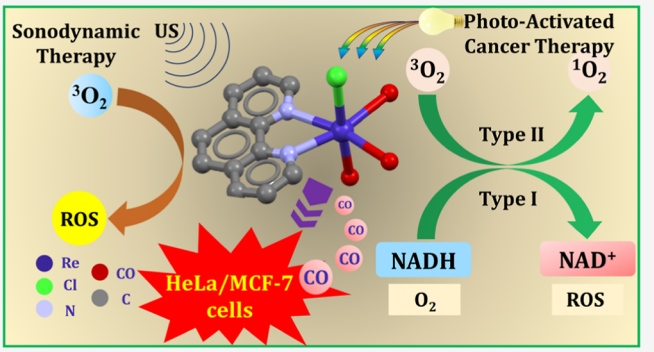

INTRODUCTION

The widespread use of platinum-based chemotherapeutics for cancer treatment is now suffering from several drawbacks, such as side effects and drug resistance.[1−3] Over the last few decades, researchers have developed new treatment modalities with new anticancer compounds to overcome the drawbacks of the clinical Pt(II)-based cancer drugs.[4−8] In this regard, selective activation of a cancer drug at the cancer site is proven to be effective in reducing drug side effects.[7−9] Based on this concept, cancer treatment modalities like photoactivated cancer therapy (PACT) and sonodynamic therapy (SDT) were developed.[10−13] Metal complexes showed positive response as the cancer prodrugs in PACT and SDT.[14−17] Several 3d−5d metal (such as VO(II), Zn(II), Ru(II), Ir(III), Pt(IV), and Os(II), etc.) complexes presented light-triggered anticancer activities through different modes of action.[18−23] Recently, metal complexes are also attracting attention as sonosensitizers in SDT.[24] A cyanine-based Pt(II) complex is reported to induce ferroptotic cancer cell death upon ultrasound exposure.[24] Re(I)-tricarbonyl complexes have attracted notable attention as PACT agents due to their ROS generation abilities and CO-releasing properties on light exposure.[25−30] ROS generation and CO-releasing abilities of Re(I)-tricarbonyl complexes made them good dual-action PACT agents.[26,27] Wilson and co-workers have reported the 365 nm light-activated anticancer activity of Re(I) complexes via the combined effect of CO release, $^1O_2$ generation, and rhenium-containing photoproducts.[26] Gasser et al. have shown the ROS-mediated apoptosis/necrosis of HeLa cells induced by Re(I)-tricarbonyl complexes upon 350 nm light exposure.[30] In another report, the Gasser group showed cell-specific 350 nm light-triggered anticancer activity via $^1O_2$ generation-mediated DNA damage by a neuropeptide, bombesin, conjugated Re(I) tricarbonyl.[31] Pan et al. have reported dinuclear phosphorescent Re(I)-tricarbonyl complexes showing 425 nm light-induced phototoxicity by lysosomal membrane permeabilization and ROS production.[28] Maisuls et al. have reported a dppz-Re(I)-tricarbonyl complex showing 365 nm light-triggered cancer cell death via ROS-induced DNA damage.[32] The Meggers group has explored the potential of Re(I) tricarbonyl to achieve visible-light anticancer activity.[33] Importantly, most of the reported Re(I)-tricarbon-

Received: December 31, 2023
Revised: March 23, 2024
Accepted: March 29, 2024
Published: April 11, 2024

https://doi.org/10.1021/acs.jmedchem.3c02485
J. Med. Chem. 2024, 67, 6537−6548

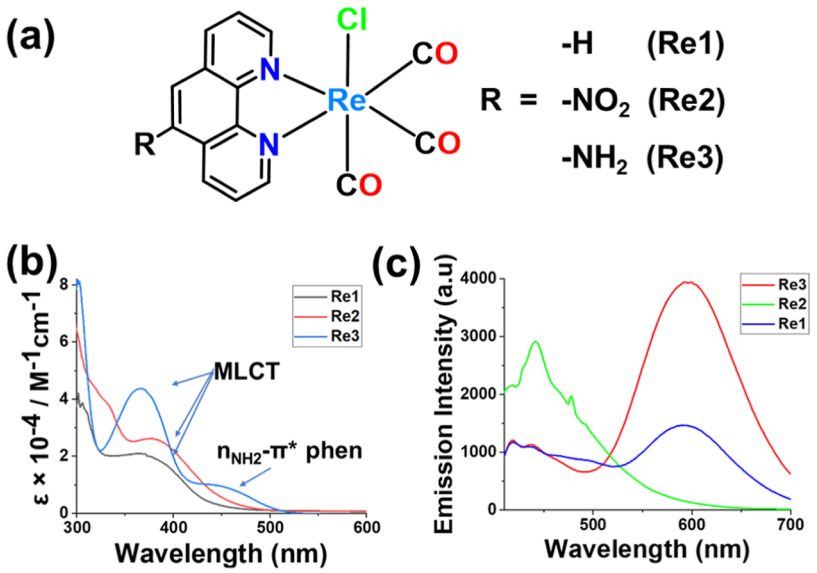

Figure 1. (a) Structure of complexes **Re1**−**Re3**. (b) Absorption spectra of **Re1**−**Re3** in DMSO/H_2O (10:90 v/v) solution. (c) Emission spectra of complexes **Re1**−**Re3** in DMSO/H_2O (10:90 v/v) solution (20 μM, λ_{ex} = 370 nm for **Re1**/**Re3** and 390 nm for **Re2**).

yl-based PACT agents were excited with UV light to achieve anticancer activities and, thus, are not highly suitable for clinical applications.[26−32] Limited report is available for high wavelength light-induced anticancer effects, but their activity was due to the presence of the porphyrin moiety, not the Re(I) core.[34] Thus, Re(I)-tricarbonyl complexes, which can show visible-light-induced anticancer activity, are needed to broaden the scope of Re(I) tricarbonyls in clinical PACT applications.

The low tissue penetration power of visible light (except red light) compromises the overall potential of PACT.[12,16] Recently, SDT with ultrasound as the drug stimulus has evolved to overcome this limitation of PACT.[8,15,24,35] Of late, our group and Zhang's group have shown that ultrasound can also trigger anticancer activities out of Re(I) tricarbonyls by releasing CO gas and ROS generation, establishing the usefulness of Re(I) tricarbonyls in SDT.[36] Till today, a comparative study between SDT and PACT with Re(I)-tricarbonyl complexes is missing. Such a study could provide information about the SDT and PACT performances of Re(I)-tricarbonyl complexes under ultrasound and light exposure, respectively. A comparative study could also indicate the possibility of multimodal cancer therapy combining SDT and PACT.

In this work, we have used simple Re(I)-tricarbonyl complexes, viz., [Re(phen)$(CO)_3$Cl] (**Re1**), [Re(phen-NO_2)-$(CO)_3$Cl] (**Re2**), and [Re(phen-NH_2)$(CO)_3$Cl] (**Re3**), where phen = 1,10-phenanthroline; phen-NO_2 = 5-nitro-1,10-phenanthroline; phen-NH_2 = 5-amino-1,10-phenanthroline, to get visible light-assisted PACT and SDT.[37−43] We also compared the anticancer activity of these complexes in the presence of ultrasound and visible light. Important findings of this work comprise: (i) both light and ultrasound can activate the Re(I)-tricarbonyl complexes to induce apoptosis via ROS generation and NADH oxidation. (ii) Cytotoxicity under ultrasound was a bit less than light, but ultrasound with high tissue penetration might be useful for further *in vivo* studies, which will be the topic of our future investigation.

RESULTS AND DISCUSSION

Synthesis and Structural Analysis. Complexes **Re1**−**Re3** (Figure 1a) were synthesized in good yield (80−90%) by reacting stoichiometric amounts of rhenium pentacarbonyl chloride, [$Re(CO)_5Cl$], and 1, 10-phenanthroline-based ligands in toluene under reflux conditions.[27,38−43] The diffusion of hexane in an acetone solution of **Re2** yielded diffraction-quality single crystals of the complex. All of the complexes were characterized with NMR, IR, HRMS, elemental analysis, and UV−vis spectroscopy (Figures S1−S12). NMR (Figures S1−S6) and elemental analysis data revealed the high purity of **Re1**−**Re3**. The HRMS of **Re1**−**Re3** in CH_3CN displayed m/z peaks corresponding to the $[M + Na]^+$ species (Figures S7−S9). The FT-IR spectra of **Re1**−**Re3** showed three bands between 1880 and 2030 cm^{-1}, confirming the presence of three facial carbonyl groups (Figures S10−S12).[27,38−42] The UV−vis spectra of **Re1**−**Re3** in 10% aq. DMSO displayed a band around 370−390 nm. These bands correspond to the Re(I)-to-ligand charge transfer, which dominates in the photophysical/chemical properties of the Re(I)-tricarbonyl complexes.[27,38−42] Complex **Re3** also displayed an additional band around 445 nm, corresponding to ligand-based n−π^* transition (Figure 1b).[39,40] **Re1** and **Re3** (in 10% aq. DMSO) on excitation at 370 nm exhibited photoluminescence with the maxima near ∼590 nm. **Re2** showed photoluminescence at ca. 440 nm under similar experimental conditions upon excitation at 390 nm (Figure 1c). The emission properties of these complexes were used to determine their internalization inside cancer cells.

X-ray Single-Crystal Structure. The crystal structure of **Re2** revealed its distorted octahedral geometry (Figure 2). **Re2** has a $P12_1/n1$ space group and monoclinic system. The crystal structure of **Re2** suggested that there were four molecules of **Re2** within the unit cell, while only one molecule was within the asymmetric unit (Figure S13). As depicted in Figure 2, Re(I) is coordinated with three CO, the N,N donor chelating ligand (5-nitro-1,10-phenanthroline), and chloride. The structure of **Re2** revealed that two of the CO were positioned at the equatorial position and one CO at the axial position, trans to Cl. Some important bond angles and lengths are listed

https://doi.org/10.1021/acs.jmedchem.3c02485
J. Med. Chem. 2024, 67, 6537−6548

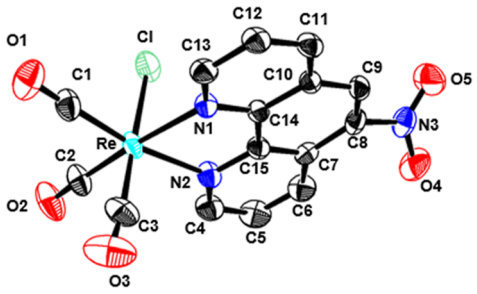

Figure 2. ORTEP view of **Re2** showing 50% probability thermal ellipsoids (CCDC = **2299334**).

in Table 1. Important crystal parameters and refinement details of **Re2** are provided in Table S1. The N1−Re−N2 angle is

Table 1. Important Bond Lengths and Bond Angles of Re2

bond lengths (Å)		bond angles (deg)			
Re−Cl	2.472(2)	Cl−Re−N1	84.1(1)	N2−Re−C3	98.1(2)
Re−N1	2.179(4)	Cl−Re−N2	81.2(1)	C8−N3−O4	118.2(5)
Re−N2	2.184(5)	Cl−Re−C1	92.3(2)	C8−N3−O5	117.3(5)
Re−C1	1.928(5)	Cl−Re−C2	92.9(2)	O4−N3−O5	124.5(6)
Re−C2	1.925(6)	Cl−Re−C3	178.3(2)	Re−N1−C14	114.6(3)
Re−C3	1.941(6)	N1−Re−N2	75.0(2)	Re−N2−C15	114.9(3)
C8−N3	1.480(8)	N1−Re−C1	97.9(2)	Re−C1−O1	178.8(6)
N3−O5	1.219(7)	N1−Re−C3	94.3(2)	Re−C2−O2	177.6(5)
N3−O4	1.218(7)	N2−Re−C2	97.6(2)	Re−C3−O3	173.9(6)

characteristically small (75.0°), in line with the previously reported structures of similar Re(I) tricarbonyls.[27,38,42] The bond angles N1−Re−Cl (81.2°) and N2−Re−Cl (84.1°) were below 90.0°, indicating that the phenanthroline moiety is little bent toward the axial Cl (Table 1).[27,38,42] The angles C1−Re−Cl (92.3°) and C2−Re−Cl (92.9°) were higher than 90°, indicating that CO groups are bent toward the axial CO (Table 1).[27,38,42] The $-NO_2$ group on phenanthroline was not planar, as was evident from the torsion angles of C7−C8−N3−O4 (∼144.8°) and C7−C8−N3−O5 (∼35.2°). The nonplanarity of the $-NO_2$ group might be due to the interaction between the nitro group oxygen and the neighboring molecule's oxygen of axial CO (Figure S13).

Computational Studies. Figure 1a shows the structures of the Re(I) carbonyl complexes investigated in this work. **Re1**−**Re3** were optimized in their singlet ground states (S_0), first excited singlet state (S_1), and in their triplet excited states (T_1) at the ωB97X-D/Def2-TZVP in DMSO.[44−46] As seen in Figure 1a, all complexes investigated are very similar in structure where Re(I) is attached to 3 CO groups, 1 Cl, and one 1,10-phenanthroline substituted at 5-C. Figure S14 shows the optimized structures, and Figure S15 and Table S2 show the FMO plots and their energies. Figure 3a reveals that for **Re1** and **Re2**, the HOMO is localized over the Re, CO, and Cl, whereas the LUMO is predominantly located on the phen ligand. In the case of **Re3**, HOMO-1 was located on the Re, CO, and Cl, HOMO was delocalized on the entire molecule, and LUMO was located on the substituted phen ligand (Figure 3a). Different vertical transition energies are given in Tables S3−S5. The oscillator strengths for each transition, represented in Tables S3−S5, show that the transitions are allowed. Furthermore, we have carried out natural transition orbital analysis on the complexes' lowest and most intense transitions (Figures S16−S18). For **Re1** and **Re2**, the red-shifted band corresponds to the HOMO → LUMO transition indicating metal-to-ligand charge transfer (^{1}MLCT). In the case of **Re3**, there was a HOMO-1 → LUMO transition with the participation of the HOMO → LUMO transition suggesting a mixture of ligand-to-ligand charge transfer (^{1}LLCT) and ^{1}MLCT. The triplet excited states (T_1) were optimized to gain insights into spin density and SOMO plot nature and to determine the energy gap between T_1 and S_0, ΔE_{ST} (Figure 3c and Table S6). The optimized singlet and triplet structures of **Re1**−**Re3** were more or less similar (Figures S19 and S20). The spin density plots of **Re1**−**Re3** in their triplet state displayed localization around the bidentate ligand and the Re atom (Figure 3b). The SOMO plots (Figure S21) suggested an ^{3}MLCT character for **Re1** and **Re2** and mixed ^{3}MLCT−^{3}LLCT in **Re3**, consistent with singlet ground states. Moreover, the energy difference ΔE_{ST} values obtained for **Re1**−**Re3** range between 2 and 2.5 eV (Table S6), and these values significantly exceeded the minimum energy required, 0.98 eV to transform $^3O_2$ into $^1O_2$ (Figure 3d).[45]

Intracellular Uptake and Cytotoxicity Assay. Adequate intracellular uptake for any cancer therapeutic is essential for *in vitro* and *in vivo* anticancer activities.[47−49] Henceforth, we examined the cellular uptake of **Re2** and **Re3** in HeLa cells after 6 h of incubation by measuring in-cell fluorescence from the complexes through flow cytometer analysis.[50,51] The flow cytometry data (Figure 4) clearly depicted that **Re2** and **Re3** internalized significantly into the HeLa cells within 6 h of incubation. The significant cellular uptake of the complexes encouraged us to study the cytotoxicity of complexes against HeLa (cervical cancer cell line), MCF-7 (breast cancer cell line) cancer cell line, and normal HEK (human embryonic kidney) cell line in both dark and after light exposure using the MTT assay.[52−55] **Re1** did not present any significant cytotoxicity against any of the tested cell lines with the presence or absence of light (400−700 nm, 5 J cm^{-2}) (Table 2). Earlier, the Mascharak group reported that **Re1** was also nontoxic against MDA-MB231 cells.[38] **Re2** and **Re3** did not produce any toxic response against HeLa and MCF-7 cells in the dark condition, even at 50 μM concentration. But, interestingly, **Re2** and **Re3** significantly decreased the cell viability of both MCF-7 and HeLa cancer cells upon light exposure in a concentration-dependent manner. The complexes **Re2** and **Re3** showed ca. 4 times higher anticancer activity in HeLa cells than in MCF-7 cells (Table 2). In contrast, dinuclear Re(I)-tricarbonyl complexes reported by Mao et al. have presented almost the same phototoxicity in both HeLa (IC_{50} = 1.8 ± 0.2 μM) and MCF-7 (IC_{50} = 2.2 ± 0.3 μM) cancer cells.[56] Both complexes showed photocytotoxicity index (ratio of dark IC_{50} to light IC_{50}) value >25 against HeLa cells, indicating their selective cancer cell-killing ability under light. More importantly, the cytotoxic effect of **Re2** and **Re3** against normal HEK cells (IC_{50} > 50 μM) was lower than cancer cells with significant SI (SI = selectivity index = ratio of IC_{50} against the normal cell to IC_{50}

https://doi.org/10.1021/acs.jmedchem.3c02485
J. Med. Chem. 2024, 67, 6537−6548

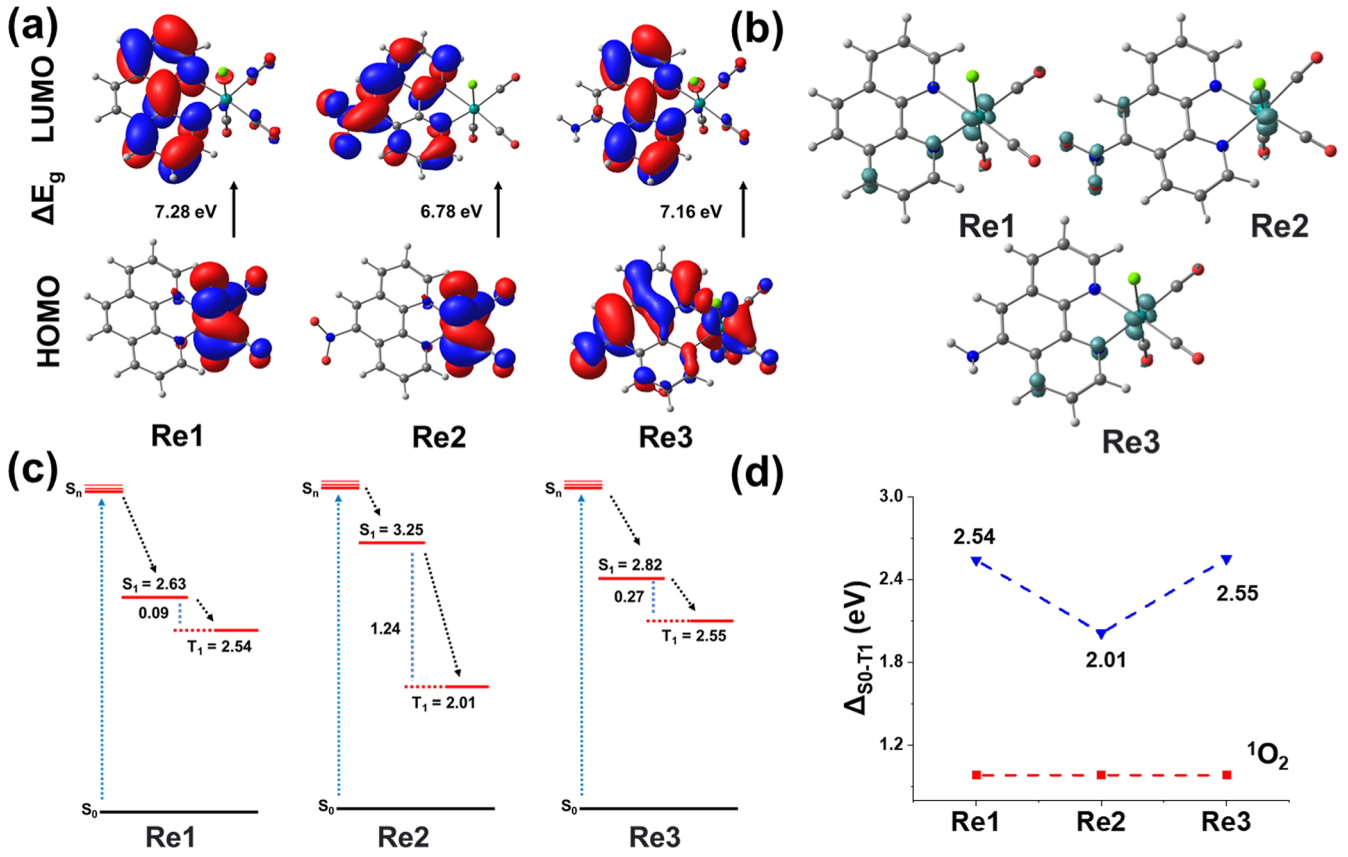

Figure 3. (a) Difference between HOMO and LUMO of complexes **Re1**−**Re3**; (b) spin density isosurface of **Re1**−**Re3** at the T_1 optimized geometries; (c) calculated energy level of lowest triplet energy (T_1) and excited singlet (S_1) levels of **Re1**−**Re3**; and (d) adiabatic singlet−triplet energy gap ($\Delta_{S_0-T_1}$) of **Re1**−**Re3**.

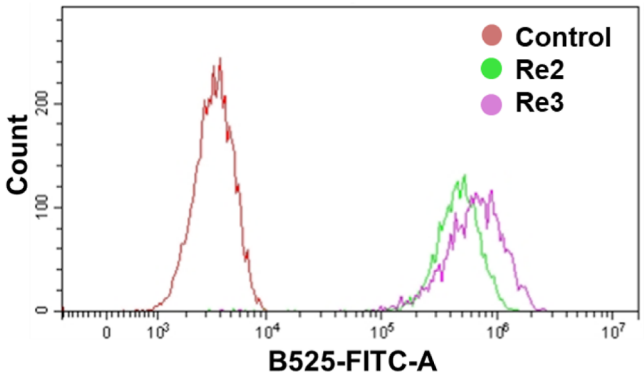

Figure 4. Flow cytometric analysis data showing the uptake of **Re2** and **Re3** (5 μM) in HeLa cells after incubation for 6 h of incubation.

against the cancer cell, SI > 25 for both **Re2** and **Re3**), indicating their high selectivity toward cancer cells.

Although photoactivated cancer therapy has offered significant therapeutic results, the low tissue penetration power of light has compromised its effect on deep-seated tumors.[8,57−60] In this regard, only the red light-absorbing photoactive molecules can be used to treat deeply buried tumors.[7,57,58] As our complexes do not have any absorption in the red light region, so might be useful for superficial cancers.[8] To overcome the limitation associated with the light's tissue penetration, the concept of SDT with ultrasound as a drug activator was introduced recently.[8,59,60] To use Re(I)-tricarbonyl complexes for deep-seated tumor therapy, ultrasound can be useful.[59,60] Ultrasound has excellent tissue-penetrating ability and thus can activate the drug even at the deep-seated tumor site.[59,60] Recently, we have shown that ultrasound can also release CO from the Re(I)-tricarbonyl complex.[59,60] To realize the efficacy of **Re1**−**Re3** in SDT, their anticancer activities were studied under ultrasound irradiation (1.5 W cm^{-2}). Moreover, we were interested in comparing the effects of light and ultrasound as drug activators. Interestingly, **Re3** showed significant anticancer activity on ultrasound exposure with the IC_{50} value ca. 5 μM against HeLa cells. Thus, **Re3** presented a marginally higher anticancer effect in the presence of visible light (IC_{50} = ca. 2 μM) than the ultrasound. The low micromolar IC_{50}s of **Re3** under light and ultrasound indicate that this complex can be used in photoactivated cancer therapy as well as in cancer SDT. The SDT performance of **Re3** is encouraging, as it can be used for deeply buried tumor as a sonosensitizer.

ROS Generation. Reactive oxygen species (ROS) production during cellular metabolism plays an important role in maintaining cellular redox harmony.[61,62,64] But any artificial increment in the intracellular ROS levels results in the damage of many cellular components, such as lipids, proteins, DNA, etc., that highly compromises regular cellular activity and leads to cell death.[61,62] ROS generation have been a pivotal mechanism in PDT as well as in SDT, which holds promising potential for anticancer effects.[59−62,64] The generation of ROS like $^1O_2$ and OH$^\bullet$ plays a vital role in cancer therapy due to their oxidative stress-mediated destruction of cancer cells.[61,62] The singlet oxygen production by photo/

https://doi.org/10.1021/acs.jmedchem.3c02485
J. Med. Chem. 2024, 67, 6537−6548

Table 2. IC_{50} Values (μM), Photocytotoxicity Index ($IC_{50\ dark}/IC_{50\ light}$), and Selectivity Index (SI, SI = $IC_{50\ normal\ cell}/IC_{50\ light,\ cancer\ cell}$) of Re1−Re3, Cisplatin, and Relevant Re(I)-Tricarbonyl Complexes

complex	HeLa					MCF-7				HEK-293
	dark	light	ultrasound	photocytotoxicity index	SI	dark	light	photocytotoxicity index	SI	dark
Re1[a]	>50	>50				>50	>50	-		>50
Re2[a]	>50	2.0 ± 0.4	>10	>25	>25	>50	9.2 ± 0.4	>5	>5	>50
Re3[a]	>50	1.9 ± 0.4	5.01	>25	>25	>50	8.8 ± 0.5	>5	>5	>50
Re−NH_2[b]	>100	17.3 ± 2.9		>6						
Re-COOH[b]	>100	9.3 ± 2.2		>10						
Re-DAPTA1[c]	>200	5.9 ± 1.4		>33.9						
Re-Cy[d]			1.99							
cisplatin[e]	71.3	68.7	1.1			69.7				

[a]This work, cells were incubated with the complexes for 6 h in the dark, followed by light (30 min, 400−700 nm, 5 J cm^{-2}) and ultrasound (10 min, 1.5 W cm^{-2}) irradiation and a further 18 h recovery time. [b]From ref 30 (light, 365 nm). [c]From ref 26 (light, 365 nm). [d]From ref 36 (US, 0.3 W cm^{-2}). [e]From ref 50 (light, 400−700 nm).

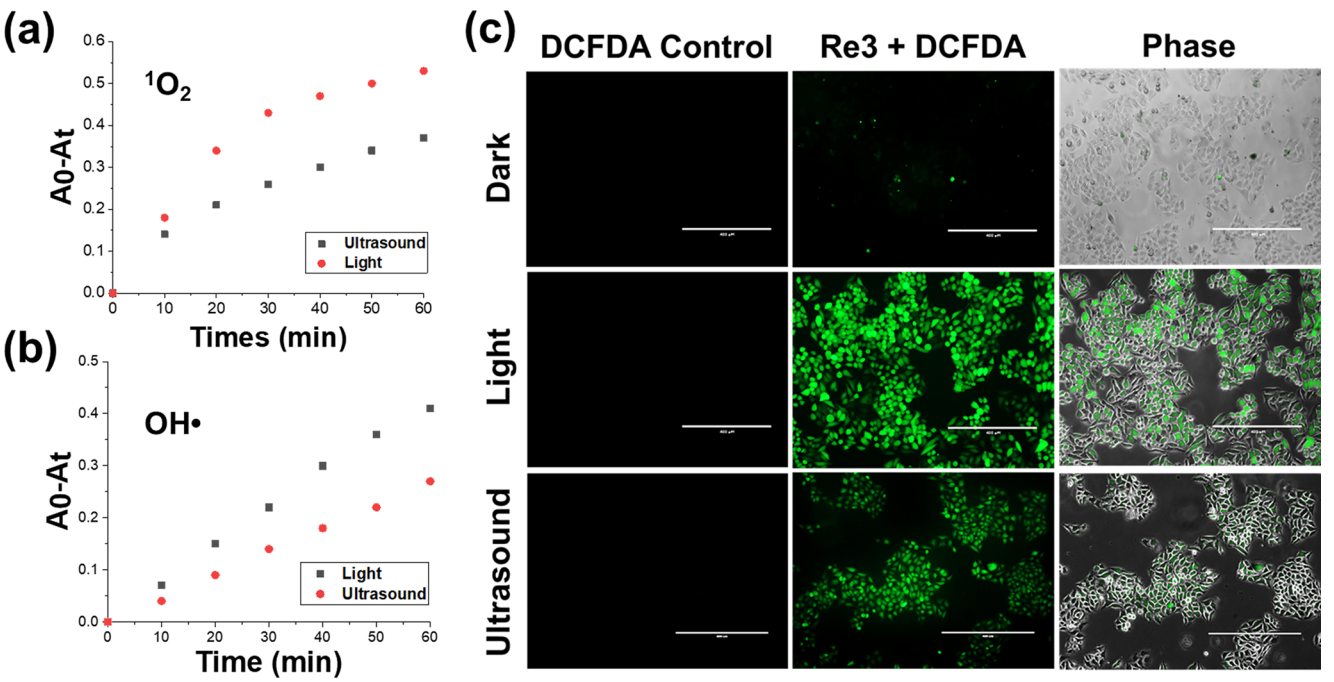

Figure 5. (a) $^1O_2$ generation induced by **Re3** (10 μM) upon light (400−700 nm, 5 J cm^{-2}) and ultrasound (1.5 W cm^{-2}) irradiation in DMSO/H_2O (2:98 v/v) solution. (b) $OH^•$ generation induced by **Re3** (10 μM) upon light (400−700 nm, 5 J cm^{-2}) and ultrasound (1.5 W cm^{-2}) irradiation in DMSO/H_2O (2:98 v/v) solution. (c) ROS generation induced by **Re3** (2 μM) upon light (400−700 nm, 5 J cm^{-2}) and ultrasound (1.5 W cm^{-2}) irradiation in HeLa cells after 30 min of incubation. Scale bar: 400 μm.

sono-sensitizers on light/ultrasound irradiation has been reported to induce cancer cell killing.[62,63] $^1O_2$ generation by photosensitizers has been an important cofactor and well-explored cell death mechanism for anticancer activity. Similarly, sonosensitizers have also been explored to produce $^1O_2$ upon ultrasound exposure. For example, Zhu et al. reported a smart sonosensitizer PpIX@HMONs-MnO_x-RGD (Arg-Gly-Asp) (named PMR) to produce $^1O_2$ by ultrasound irradiation.[63a] Similarly, Cheng and co-workers have shown $^1O_2$ generation by $H_XV_2O_5$ nanocatalysts.[63b] Ultrasound has also been reported to enhance the $^1O_2$ generation efficiency of photosensitizers. For example, Karanlık et al. have shown an increase in $^1O_2$ quantum yield by 60% upon ultrasound irradiation than light irradiation.[63c] Several metal complexes have also been reported to generate $^1O_2$ under ultrasound exposure. Recently, Xu et al. have shown the high $^1O_2$ generation efficiency by Ru(II)-based sonosensitizers.[63d] Zhang's group has explored efficient singlet oxygen production by Ir(III)-porphyrin complexes, Pt(II) complexes, and Ru(II) polypyridyl complexes.[15,17,24] In sonodynamic therapy, ultrasound waves cause cavitation within the cellular medium and form bubbles. The formed bubbles further burst violently and produce a high energy. The produced energy activates the sonosensitizer, which then most likely transfers the energy to $^3O_2$ to generate $^1O_2$.[15,17,36] As the TD-DFT calculation depicted that **Re1**−**Re3** possesses sufficient energy difference ΔE_{ST} ($\Delta_{S_0-T_1}$) to generate $^1O_2$ from $^3O_2$ (Figure 3d), the $^1O_2$ generation ability of **Re2** and **Re3** was studied using the 9,10-diphenyl anthracene (DPA) probe.[36] In the dark or in the absence of ultrasound, the absorption intensity of the DPA-based band was not changed notably in the presence of **Re2**/**Re3**, indicating that these complexes are unable to produce a significant amount of $^1O_2$ in the absence of any drug stimulus. The $^1O_2$ generation efficiency of **Re2**/**Re3** was incredibly

https://doi.org/10.1021/acs.jmedchem.3c02485
J. Med. Chem. 2024, 67, 6537−6548

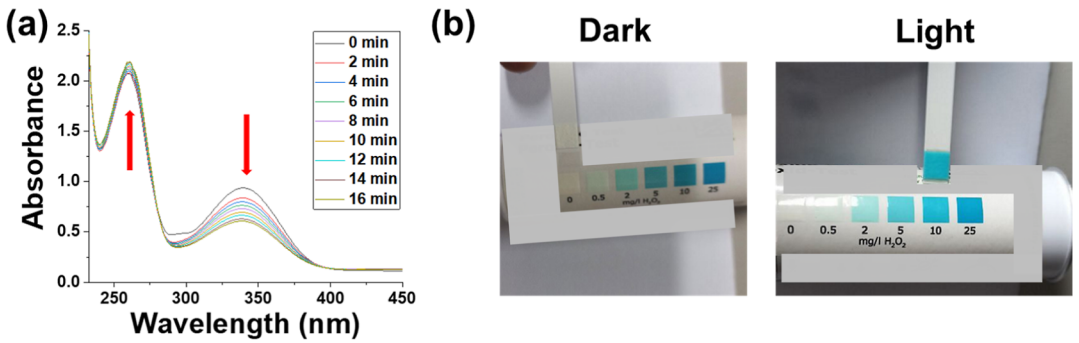

Figure 6. (a) Light-triggered NADH oxidation by **Re3** (10 μM) in DMSO-PBS (2:98 v/v) solution. (b) H_2O_2 generation by **Re3** (10 μM) in the presence of NADH upon light exposure.

increased after exposure to light (400−700 nm, 5 J cm^{-2}) and ultrasound (1.5 W cm^{-2}), as was observed from the significant decrease in the absorption intensity of the DPA-based band at 360−410 nm (Figure S22). Interestingly, **Re3** produced a higher amount of $^1O_2$ under light exposure (Figure 5a). The $^1O_2$ quantum yield of these complexes was further calculated taking $[Ru(bpy)_3]Cl_2$ as a standard (Φ_Δ^R = 0.22) in aq. DMSO.[17] The result revealed that the $^1O_2$ quantum yield for **Re3** (Φ_Δ^{Re3} = 0.24) was higher than those for **Re2** (Φ_Δ^{Re2} = 0.16) and **Re1** (Φ_Δ^{Re1} = 0.05) (Figure S23). This result indicated that **Re3** might be a better type-II PDT agent than **Re1** and **Re2**. On ultrasound exposure, the rate of DPA oxidation for $^1O_2$ generation was quantified by measuring the decrease in the time-dependent DPA-based peak (ca. 378 nm) absorbance. The DPA oxidation rate constant was observed to be 0.0068 min^{-1} for **Re3**, which was higher than those for **Re2** (0.0049 min^{-1}) and **Re1** (0.0011 min^{-1}). This observation is aligned with the photo/sonotoxicity presented by **Re2**/**Re3** and can be attributed to the higher light absorption of **Re3**. Furthermore, we examined the $OH^\bullet$ generation ability using the $OH^\bullet$ probe, methylene blue (MB).[36] Following a trend similar to $^1O_2$ production, no significant $OH^\bullet$ generation by **Re2**/**Re3** was observed under dark or without ultrasound irradiation (Figure S24), and $OH^\bullet$ generation was increased after visible light or ultrasound exposure (Figure S25). **Re3** again produced more $OH^\bullet$ compared to **Re2** (Figure 5b). Thus, these complexes show anticancer activity under light via both type-I and type-II PDT pathways. It is important to mention that, although several Re(I)-tricarbonyl complexes are reported to produce $^1O_2$ upon light or ultrasound exposure,[36,59] $OH^\bullet$-generating Re(I)-tricarbonyl complexes are not reported yet.

Furthermore, the ROS generation ability of **Re2** and **Re3** in the HeLa cells was visualized using the fluorescent probe, DCFDA (2,7-dichlorodihydrofluorescein diacetate), and fluorescence microscopy.[61−63] In this approach, the generated ROS is known to transform the nonfluorescent DCFDA into the highly fluorescent 2′,7′-dichlorofluorescein (DCF).[61−63] Complexes **Re2** and **Re3** showed significant ROS generation at their respective IC_{50} concentrations only upon light and ultrasound exposure (Figures 5c and S26−S28). Importantly, in the absence of drug stimuli (light or ultrasound), **Re2** and **Re3** were unable to generate observable ROS (Figure S26), indicating that the **Re2**/**Re3** + light/ultrasound combination considerably enhanced ROS generation (DCF green fluorescence) in HeLa cells and promoted cell death via oxidative stress.

Oxidation of NADH to NAD^+. In addition to serving as a crucial coenzyme in more than 400 oxidoreductases in live cells,[65,66] NADH is recognized as the main e^- source in the mitochondrial electron transport chain (ETC).[65−72] Moreover, the overall in-cell NADH level is higher in cancerous cells than in normal cells to ensure high cell proliferation.[69,73] Henceforth, any artificial depletion in NADH in cancer cells can provide a multitargeting anticancer activity.[65−72] Recently, the Sadler group, Huang group, and our group have successfully demonstrated that in-cell artificial oxidation of NADH/NAD(P)H by metal complexes leads to cell death.[65−72] Motivated by the appealing excited-state photochemistry and ROS generation ability of **Re3**, we investigated the light-triggered oxidation of NADH to NAD^+. The gradual decrease in the intensity of the NADH-based band at ca. 339 nm and subsequent increase in the intensity of NAD^+ based at ca. 260 nm indicated the oxidation of NADH to NAD^+ (Figure 6a).[65−72] It was found that **Re3** (TON = 4.9, TOF = 16.3 h^{-1}) significantly oxidizes NADH to NAD^+ under the influence of visible light (400−700 nm, 5 J cm^{-2}) (Figure 6a) and does not exhibit any effect without light (Figure S29). NADH oxidizing ability of **Re3** on light irradiation was supported by the excited-state redox potential calculation. At the excited state, the reduction potential of **Re3** ($[\mathbf{Re3}^*]^0/[\mathbf{Re3}]^-$ = +0.83 V) (Table S7) was higher than NADH ($[NAD]^+/[NADH]$ = +0.32 V).[66] Therefore, NADH transferred electrons to **Re3*** and was converted into $NADH^{\bullet+}$, which further converted O_2 to H_2O_2. H_2O_2 production was detected using peroxide test strips (Figure 6b). A similar mechanism is also reported with Ir(III) complexes.[65−68] Overall, the above results indicated that the photocytotoxicity of **Re3** could be a combined effect of type-I and type-II ROS generation mechanisms and in-cell NADH oxidation. It is important to mention here that the reported metal complexes showing NADH oxidation are either Ru(II) or Ir(III) complexes, and this is the first Re(I)-tricarbonyl complex showing NADH oxidation.

CO Release. Several reports suggested that Re(I)-tricarbonyl complexes can release CO upon light or ultrasound irradiation.[26,27,36−38] For example, Wilson et al. and Mascharak et al. have established that Re(I) tricarbonyls can serve as CO-releasing molecules under the influence of light.[26,27,38] The Wilson group recently reported the enhanced cytotoxicity of Re(I) tricarbonyls due to CO release in photoactivated cancer therapy.[26] Furthermore, Zhang et al. and our group proved that CO can be released from Re(I)-tricarbonyl complexes with ultrasound exposure to enhance anticancer activities.[36,59] Therefore, the release of CO from **Re3** was investigated by a UV−vis study under the influence of visible light and

https://doi.org/10.1021/acs.jmedchem.3c02485
J. Med. Chem. 2024, 67, 6537−6548

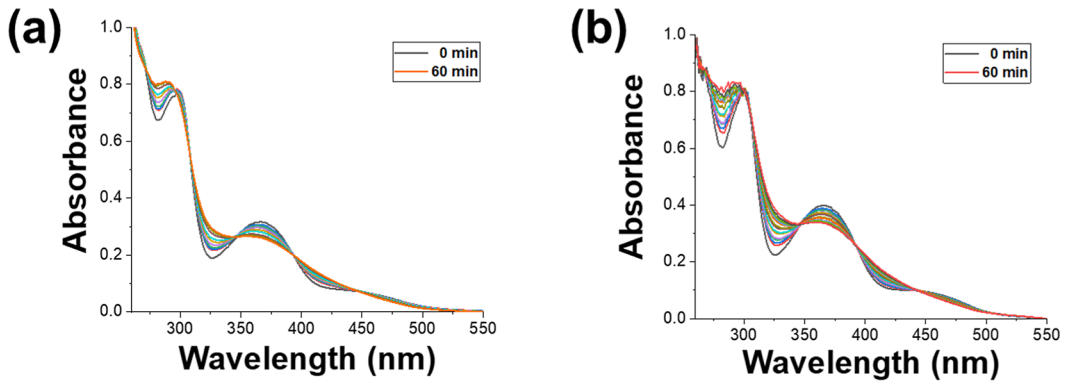

Figure 7. Change in UV−vis spectra reflecting CO release from **Re3** (15 μM) in DMSO-PBS (2:98 v/v) solution (pH 7.4) over a period of 60 min under (a) visible-light irradiation and (b) ultrasound irradiation.

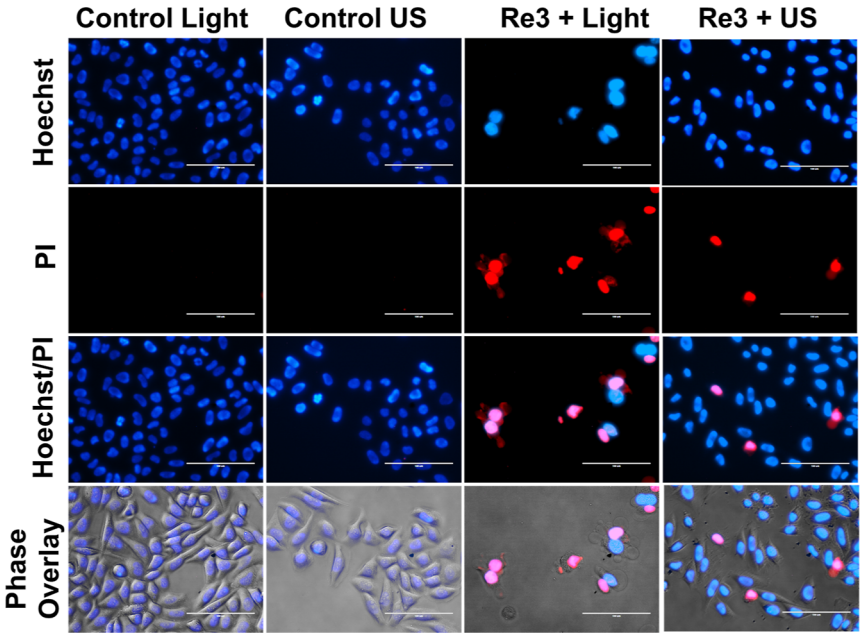

Figure 8. Light/ultrasound-triggered apoptotic cell death of HeLa cells induced by **Re3** (2 μM) probed by Hoechst and PI. Scale bar: 100 μm.

ultrasound. The change in UV−vis absorption spectra taken in PBS buffer (pH 7.4) with time indicated the loss of CO with light exposure (Figure 7a). The presence of well-defined isosbestic points in the UV−vis spectra of **Re3** indicated the CO release upon visible-light exposure.[26,27,38] CO release from **Re1** was reported by the Mascharak group with high-energy light (<315 nm).[38] Possessing an absorption maximum similar to that of **Re1**, CO release from **Re2** might be achieved with higher energy UV light. A similar observation was also found with the change in UV−vis spectra under the influence of ultrasound (Figure 7b), indicating that **Re3** can release CO under the influence of light and ultrasound. Furthermore, this result was also complimented by IR spectroscopy, where the intensity of the **Re3**-based IR peaks between 1880 and 1920 cm^{-1} corresponding to the CO stretching frequency decreased significantly upon light and ultrasound exposure (Figure S30). The computed energy difference between the final and initial states of the CO release is shown in Figure S31. For **Re3**, the ΔG between these two states in S_0 PES is 5.99 eV, whereas the ΔG between these two states in T_1 PES is 4.16 eV at the ωB97X-D/def2-TZVP//ωB97X-D/def2-SVP level of theory. These energy differences show that the reaction is endothermic and gives an estimate of the reaction barrier. The irradiation of light or ultrasound provided this amount of energy.

Apoptosis Study. The increment in cytotoxicity and ROS generation ability of **Re2** and **Re3** after light/ultrasound irradiation prompt further investigation into the cell death mechanism caused by the (**Re2**/**Re3**) + light/ultrasound combination against HeLa cells. Hoechst/PI dual staining was used to determine the cell death mechanism.[63,74,75] Hoechst 33342 dye is known to probe the nuclei of both apoptotic and live cells as it produces light-blue emission with live cells' nuclei and strong blue emission upon binding with the nuclei of apoptotic cells.[74] The other dye, PI (propidium iodide), stains the nuclei of dead or dying cells and produces bright-red fluorescence.[75] As shown in Figure 8, after **Re2**/**Re3** (at their respective IC_{50} concentration) + light/ultrasound treatment, HeLa cells' nuclei showed blue emission with Hoechst and red fluorescence with PI, indicating toward apoptotic cell death mechanism for both photoactivated cancer therapy and SDT remaining inactive without drug stimuli (Figures S32−S34).[74] Moreover, the nuclei, as well as the cells, seemed to be rounded up. The condensed nuclei were noted to be bright. Therefore, it can be implied that **Re2** and **Re3** induced

https://doi.org/10.1021/acs.jmedchem.3c02485
J. Med. Chem. 2024, 67, 6537−6548

apoptosis in HeLa cells under light or ultrasound exposure. A similar observation was also found with Re(I) complexes reported by Wilson and co-workers, showing the light-triggered apoptosis as the cell death mechanism.[26] In contrast, a cyanine-based Re(I) tricarbonyl induced ferroptosis under ultrasound exposure.[36,59]

CONCLUSIONS

In summary, we reported the synthesis and characterization of three Re(I)-tricarbonyl complexes (**Re1**−**Re3**). The crystal structure of complex **Re2** confirmed the distorted octahedral geometry of the complexes. The emission properties of **Re2** and**Re3** were used to determine their internalization inside cancer cells. The TD-DFT data indicated that the energy gap between the triplet excited state and the ground state ($\Delta E_{S_0-T_1}$) is more than 0.98 eV, which is required to produce $^1O_2$. The visible band at 400−500 nm for **Re3** was helpful in obtaining visible light-assisted $^1O_2$ generation, CO release, and anticancer responses. **Re2** and **Re3** were nontoxic (IC_{50} > 50 μM) in the absence of light to HeLa cells but potentially induced apoptosis (IC_{50} = ca. 2.0 μM) on visible-light exposure. **Re2** did not display efficient cytotoxic effects upon ultrasound exposure, while **Re3** still displayed cytotoxicity on ultrasound exposure (IC_{50} = 5.0 μM). **Re3** has a high photocytotoxicity index (>25), suggesting selective anticancer activity efficacy under visible-light exposure. Importantly, against normal HEK cells, **Re2** and **Re3** did not produce any noticeable toxicity, indicating their tumor-targeting anticancer potential. Interestingly, **Re3** was not only able to generate ROS but also induced NADH to NAD^+ photo-oxidation. To the best of our knowledge, NADH photo-oxidation has been achieved with the Re(I) complex for the first time here. Moreover, **Re3** released CO upon ultrasound and light exposure. The CO release profile of **Re3** indicated the necessity of light/ultrasound as a trigger. The released CO possibly contributed to the overall cytotoxicity of **Re3**. Considering the above-mentioned mechanistic evidence, this study indicates the ability of **Re3** to act as multitargeting and multifunctional (ROS generation, NADH photo-oxidation, and CO release) anticancer agents under the influence of light or ultrasound. Even though **Re3** presented better activity under visible light than ultrasound, it can still be useful for superficial carcinomas only due to visible light's poor tissue penetration ability. However, the activation of **Re3** with ultrasound might be used to treat buried tumors due to ultrasound's deep tissue-penetration ability.

EXPERIMENTAL SECTION

General Synthetic Procedure. 5-nitro-1,10-phenanthroline (phen-NO_2) and 5-amino-1,10-phenanthroline (phen-NO_2) were synthesized according to the method described in the literature (Scheme S1).[27] 1.0 equiv of phen-based ligands [1,10-phenanthroline (in **Re1**), 5-nitro-1,10-phenanthroline (in **Re2**), and 5-amino-1,10-phenanthroline (in **Re3**)] and 1.0 equiv of $Re(CO)_5Cl$ were dissolved in 15−20 mL of toluene (Scheme S1).[27] The reaction mixture was refluxed for 2 h under inert conditions. After 1−1.5 h, precipitation started. The precipitated complexes were filtered, washed with hexane and Et_2O, and dried in a vacuum over P_4O_{10}. The complexes were recrystallized from a DCM−ethanol mixture. The purity of complexes was determined by elemental analysis and NMR data, and the result indicated >95% purity.

*Complex **Re1***. Yellow powder, 85% yield. $C_{15}H_8ClN_2O_3Re$ (MW = 485.89 g/mol) calcd: C, 37.08; H, 1.66; N, 5.77. Found: C, 37.21; H, 1.73; N, 5.84. **Re1** has >95% purity. HRMS (m/z for $[M + Na]^+$): calcd, 508.9679; found, 508.9658. UV−visible spectral data were recorded in 10% aq. DMSO where λ_{max} = 372 nm ($\varepsilon = 2.08 \times 10^4$ M^{-1} cm^{-1}). ^1H NMR (500 MHz, DMSO-d_6): δ 9.45 (dd, J = 5.0, 1.4 Hz, 2H), 8.99 (dd, J = 8.3, 1.4 Hz, 2H), 8.35 (s, 2H), 8.13 (dd, J = 8.2, 5.0 Hz, 2H). IR (cm^{-1}): 2016 (s, sh, and assym CO), 1935 (s, sh, and assym CO), 1890 (s, sh, and assym CO), 1423 (m and sh), 851 (s and sh) [m, medium; s, strong; br, broad; sh, sharp; assym, asymmetric].

*Complex **Re2***. Orange solid, 82% yield. $C_{15}H_7ClN_3O_5Re$ (MW = 530.89 g/mol) calcd: C, 33.94; H, 1.33; N, 7.92. Found: C, 34.16; H, 1.36; N, 7.83. **Re2** has >95% purity. HRMS (m/z) $[M + Na]^+$: calcd, 553.9529; found, 553.9536. $[M + CH_3CN-Cl]^+$: calcd, 537.0209; found, 537.0206. $[M - Cl]^+$: calcd, 495.9943; found, 495.9937. UV−visible spectral data were recorded in 10% aq. DMSO where λ_{max} = 328 ($\varepsilon = 3.85 \times 10^4$ M^{-1} cm^{-1}), 382 ($\varepsilon = 2.59 \times 10^4$ M^{-1} cm^{-1}). ^1H NMR (500 MHz, DMSO-d_6): δ 9.60 (dd, J = 11.9, 5.1 Hz, 2H), 9.41 (d, J = 2.6 Hz, 1H), 9.33 (dd, J = 8.6, 2.1 Hz, 1H), 9.21 (dt, J = 8.1, 1.8 Hz, 1H), 8.30−8.19 (m, 2H). IR (cm^{-1}): 2020 (s, sh, and assym CO), 1918 (s, sh, and assym CO), 1893 (s, sh, and assym CO), 1537 (m and sh), 1418 (m and sh), 1329 (b and sh).

*Complex **Re3***. Reddish solid, 64% yield. $C_{15}H_9ClN_3O_3Re$ (MW = 500.91 g/mol) calcd: C, 35.97; H, 1.81; N, 8.39. Found: C, 36.21; H, 1.89; N, 8.31. **Re3** has >95% purity. HRMS (m/z) $[M + Na]^+$: calcd, 523.9788; found, 523.9783. $[M - Cl]^+$: calcd, 466.0201; found, 466.0196. UV−visible spectral data were recorded in 10% aq. DMSO where λ_{max} = 367 nm ($\varepsilon = 4.37 \times 10^4$ M^{-1} cm^{-1}), 450 nm ($\varepsilon = 0.95 \times 10^4$ M^{-1} cm^{-1}). ^1H NMR (500 MHz, DMSO-d_6): δ (ppm) 9.39 (dd, J = 5.1, 1.2 Hz, 1H), 9.13 (dd, J = 8.5, 1.3 Hz, 1H), 8.94 (dd, J = 4.9, 1.3 Hz, 1H), 8.50 (dd, J = 8.4, 1.2 Hz, 1H), 8.07 (dd, J = 8.5, 5.1 Hz, 1H), 7.80 (dd, J = 8.4, 4.9 Hz, 1H), 7.07 (s, 1H), 6.90 (s, 2H). IR (cm^{-1}): 2021 (s, sh, and assym CO), 1895 (s, sh, and assym CO), 1634 (m and sh), 1432 (m and sh), 1313 (b and sh).

DFT Calculation. The DFT and TD-DFT calculations were carried out on neutral Re complexes with the Gaussian 16 revision A.03 quantum chemistry package. For all calculations, the ωB97X-D/Def2-TZVP level of theory was used using the CPCM solvation model in DMSO. The ground-state (S_0) geometry of the complexes was carried out using restricted DFT, the S_1 geometry using TD-DFT and the first excited triplet-state (T_1) geometry using unrestricted DFT. The optimized S_0 and T_1 structures were confirmed to local minima at the same computational level. Natural transition orbitals (NTOs) and frontier molecular orbitals (FMOs) were generated at the same level of theory. The redox as well as the photoredox potentials of **Re1**−**Re3** were evaluated using the Born−Haber cycle. The standard potentials at 293 K were determined from the solvated free energies using

$$E^0_{abs} = -\frac{\Delta G_{red}(sol)}{nF} - 0.03766$$

where n = 1 (no. of free electrons), ΔG_{red}(sol) is the Gibbs free energy, and F is the Faraday constant for the solvated reduction half-reaction, and they were calculated vs Ag/AgCl.

NADH Oxidation. Reactions between **Re3** (10 μM) and NADH (140 μM) in DMSO-PBS (2:98 v/v) solution were monitored by UV−vis spectroscopy at ambient temperature in the dark or light irradiation.[65] The turnover number (TON) and turnover frequency (TOF) of catalysis were calculated using the following equations

$$[NAD^+] = [Abs(339\ nm)_i - Abs(339\ nm)_f]/Abs(339\ nm)_i \times [NADH]$$

$$TON = [NAD^+]/[\mathbf{Re3}]$$

$$TOF = TON/time\ (h)$$

Detection of H_2O_2 Generation. During the reaction of **Re3** (10 μM) with NADH (140 μM) in the DMSO-PBS solution (2:98 v/v) at ambient temperature in the dark or after light (400−700 nm, 5 J cm^{-2}) exposure for 16 min, H_2O_2 was detected by Quantofix peroxide test sticks.[65] The H_2O_2 generation level in the solution can be

https://doi.org/10.1021/acs.jmedchem.3c02485
J. Med. Chem. 2024, 67, 6537−6548

correlated to the color change from white to blue (of the test sticks), indicating 0−25 mg/L amount of H_2O_2.

$^1O_2$ Generation. The $^1O_2$ generation was measured using the DPA probe upon light or ultrasound irradiation.[36] In brief, a DMSO/H_2O (2:98 v/v) solution containing 10 μM of **Re1**−**Re3** and 0.3 μg/mL of DPA was monitored by UV−vis spectroscopy on different intervals of ultrasound (1.5 W cm^{-2}) or light (400−700 nm, 5 J cm^{-2}) exposure. The absorbance of the ca. 378 nm peak was monitored for $^1O_2$ generation. The $^1O_2$ quantum yields (Φ_Δ) for **Re1**−**Re3** were determined by following equation

$$\Phi_\Delta{}^S = \Phi_\Delta{}^R \times (M_S/M_R)$$

where "M" denotes the linear fit slope of the DPA-based peak at 378 nm vs the time interval. "S" denotes the samples, and "R" denotes the standard ($[Ru(bpy)_3]Cl_2$).

Detection of OH$^\bullet$ Generation. The production of hydroxyl radical (OH$^\bullet$) in solution was detected using MB as the OH$^\bullet$ probe.[36] The reaction between 10 μM **Re1**−**Re3** and 1 μg/mL MB in DMSO/H_2O (2:98 v/v) solution was monitored by UV−vis spectroscopy after different intervals of ultrasound (1.5 W cm^{-2}) and visible-light (400−700 nm, 5 J cm^{-2}) irradiation.

Cytotoxicity Assay (Both Light and Ultrasound). The cytotoxicity assay of **Re1**−**Re3** has been performed against HeLa cells (cervical carcinoma), MCF-7 cells (mammalian breast adenocarcinoma), and HEK cells (normal cell line). In brief, 10,000 cells/well were seeded in 3 different (one for light exposure, second one for dark conditions, and third one for ultrasound exposure) 96-well cell culture plates and incubated overnight for adherence. After incubation, the cells were treated at various concentrations of each drug (500 nM, 750 nM, 1 μM, 5 μM, 10 μM, 20 μM, and 50 μM) and kept for a further 6 h incubation. Thereafter, the drug-containing medium was discarded and 100 μL PBS was added into each well of all treated 96-well plates. One of those plates was exposed to light (400−700 nm, 5 J cm^{-2}) for 30 min, and subsequently, one was kept in a dark condition and the third one was irradiated with ultrasound (for 10 min). After 30 min, PBS was removed from both plates, and a fresh complete medium was added and incubated for another 18 h. Finally, the medium was discarded, and the fresh MTT-containing medium was added to each well. After 2 h of incubation, the MTT-containing medium was removed, and 100 μL DMSO was added into each well and further incubated for 0.5 h. Thereafter, absorbance was recorded in a multiplate reader at 570 nm.

ROS Generation (Both Light and Ultrasound). The assay was performed by seeding 0.5 × 10^5 HeLa cells/well in 12-well cell culture plates followed by treatments with compounds **Re2** and **Re3** at their respective IC_{50} value concentration and incubated for 6 h. A fresh PBS was added to each well after discarding the drug-containing medium, and one plate was exposed to light, another one was irradiated with ultrasound, and subsequently, one was kept in dark condition. After light and ultrasound irradiation, PBS was removed, and fresh DMEM was added to each plate and incubated for another 18 h. The cells underwent a PBS wash, followed by addition of 10 μM DCFDA, followed by incubation at 37 °C for 0.5 h. Finally, images were photographed in a fluorescent microscope under green channels and phase contrast at 100× magnification.

Apoptosis Study by Hoechst/PI Dual Staining (Both Light and Ultrasound). To investigate the nuclear morphology changes after **Re2** and **Re3** treatments, we performed Hoechst 33342/PI dual staining. For this, 50,000 HeLa cells/well were seeded in 12-well plates supplemented with complete DMEM followed by treatments with **Re2** and **Re3** at their respective IC_{50} value concentration and incubated for 6 h. Then, the drug-containing medium was discarded, fresh PBS was added to each well, and one plate was exposed to light (400−700 nm, 5 J cm^{-2}), another one was irradiated with ultrasound, and one was kept in dark condition. After light and ultrasound irradiation, PBS was removed, and fresh DMEM was added to each plate and incubated for another 18 h at 37 °C in a humidified 5% CO_2 incubator. Finally, staining with 10 μg/mL PI and 10 μg/mL Hoechst 33342 was done, and images were captured in a fluorescent microscope in phase contrast, red, and blue channels at 400× magnification.

■ ASSOCIATED CONTENT

Supporting Information

The Supporting Information is available free of charge at https://pubs.acs.org/doi/10.1021/acs.jmedchem.3c02485.

Crystal data parameters, FMO energies, singlet−singlet/triplet transition energies, adiabatic singlet−triplet splitting energies, computed redox potentials, characterization data (^{1}H and ^{13}C NMR, HRMS, FT-IR), unit cell packing, FMOs, NTOs, HOMO−LUMO energy gap, optimized geometries in S_1 and T_1, SOMOs, $^1O_2$ generation, OH$^\bullet$ generation, in-cell ROS generation, NADH oxidation, and confocal images for cell death mechanism (PDF)

Crystallographic data for complex **Re1**−**Re3** (CIF)

Check CIF/PLATON report (PDF)

Molecular formula strings of **Re1**−**Re3** (CSV)

■ AUTHOR INFORMATION

Corresponding Authors

Samya Banerjee − *Department of Chemistry, Indian Institute of Technology (BHU), Varanasi, Uttar Pradesh 221005, India*; orcid.org/0000-0003-4393-4447; Email: samya.chy@itbhu.ac.in

Biplob Koch − *Department of Zoology, Institute of Science, Banaras Hindu University, Varanasi, Uttar Pradesh 221005, India*; Email: biplob@bhu.ac.in

Tumpa Sadhukhan − *Department of Chemistry, SRM Institute of Science and Technology, Kattankulathur, Tamil Nadu 603203, India*; Email: tumpas@srmist.edu.in

Authors

Rajesh Kushwaha − *Department of Chemistry, Indian Institute of Technology (BHU), Varanasi, Uttar Pradesh 221005, India*

Virendra Singh − *Department of Zoology, Institute of Science, Banaras Hindu University, Varanasi, Uttar Pradesh 221005, India*

Silda Peters − *Department of Chemistry, SRM Institute of Science and Technology, Kattankulathur, Tamil Nadu 603203, India*

Ashish Kumar Yadav − *Department of Chemistry, Indian Institute of Technology (BHU), Varanasi, Uttar Pradesh 221005, India*

Complete contact information is available at: https://pubs.acs.org/10.1021/acs.jmedchem.3c02485

Author Contributions

R.K. and A.K.Y. synthesized and characterized the complexes. V.S. performed the biological assays. R.K. performed ROS generation and NADH photo-oxidation studies. S.P., R.K., and T.S. performed the TD-DFT calculations. S.B., B.K., and T.S. designed the studies and formulated the concept and overall project. The manuscript was written through the contributions of all authors. All authors have approved the final version of the manuscript.

Notes

The authors declare no competing financial interest.

https://doi.org/10.1021/acs.jmedchem.3c02485
J. Med. Chem. 2024, 67, 6537−6548

■ ACKNOWLEDGMENTS

We thank SERB (SRG/2022/000030), the Government of India, and BRNS (54/14/08/2022-BRNS-R) for financial support. R.K. and A.K.Y. thank the Ministry of Education, the Government of India, for the Prime Minister's Research Fellowship. B.K. acknowledges the Indian Council of Medical Research, New Delhi, India, for providing financial support (no. 5/13/36/2022-NCD-111) and Banaras Hindu University for providing funding under the IoE scheme (file no. R/Dev/D/IoE/Incentive/2021-22/32449). We thank the high-performance computing facilities at IIT BHU and SRMIST. We sincerely thank Sukanta Saha for his help in solving the X-ray structure and Mr. Ashish Kumar Maurya for laboratory management.

■ ABBREVIATIONS

CO, carbon monoxide; DCFDA, 2,7-dichlorodihydrofluorescein diacetate; DMEM, Dulbecco's modified Eagle's medium; DPA, 9,10-diphenyl anthracene; LLCT, ligand-to-ligand charge transfer; MB, methylene blue; MLCT, metal-to-ligand charge transfer; MTT, 3-(4,5-dimethylthiazol-2-yl)-2,5-diphenyltetrazolium bromide; NTO, natural transition orbital; PACT, photoactivated cancer therapy; SDT, sonodynamic therapy; TOF, turnover frequency

■ REFERENCES

(1) Kelland, L. The resurgence of platinum-based cancer chemotherapy. *Nat. Rev. Cancer* **2007**, *7*, 573−584.
(2) Oun, R.; Moussa, Y. E.; Wheate, N. J. The side effects of platinum-based chemotherapy drugs: a review for chemists. *Dalton Trans.* **2018**, *47*, 6645−6653.
(3) Zhou, J.; Kang, Y.; Chen, L.; Wang, H.; Liu, J.; Zeng, S.; Yu, L. The Drug-Resistance Mechanisms of Five Platinum-Based Antitumor Agents. *Front. Pharmacol* **2020**, *11*, 343.
(4) Charmsaz, S.; Collins, D. M.; Perry, A. S.; Prencipe, M. Novel strategies for cancer treatment: highlights from the 55th IACR annual conference. *Cancers* **2019**, *11*, 1125.
(5) Debela, D. T.; Muzazu, S. G.; Heraro, K. D.; Ndalama, M. T.; Mesele, B. W.; Haile, D. C.; Kitui, S. K.; Manyazewal, T. New approaches and procedures for cancer treatment: Current perspectives. *SAGE Open Med.* **2021**, *9*, 205031212110343.
(6) Baudino, T. A. Targeted Cancer Therapy: The Next Generation of Cancer Treatment. *Curr. Drug Discovery Technol.* **2015**, *12*, 3−20.
(7) Gunaydin, G.; Gedik, E.; Ayan, S. Photodynamic Therapy for the Treatment and Diagnosis of Cancer−A Review of the Current Clinical Status. *Front. Chem.* **2021**, *9*, 686303.
(8) Yan, P.; Liu, L.; Wang, P. Sonodynamic Therapy (SDT) for Cancer Treatment: Advanced Sensitizers by Ultrasound Activation to Injury Tumor. *ACS Appl. Bio Mater.* **2020**, *3*, 3456−3475.
(9) Jiang, W.; Liang, M.; Lei, Q.; Li, G.; Wu, S. The Current Status of Photodynamic Therapy in Cancer Treatment. *Cancers* **2023**, *15*, 585.
(10) Paprocka, R.; Wiese-Szadkowska, M.; Janciauskiene, S.; Kosmalski, T.; Kulik, M.; Helmin-Basa, A. Latest developments in metal complexes as anticancer agents. *Coord. Chem. Rev.* **2022**, *452*, 214307.
(11) Sadanala, K. C.; Chaturvedi, P. K.; Seo, Y. M.; Kim, J. M.; Jo, Y. S.; Lee, Y. K.; Ahn, W. S. Sono-photodynamic combination therapy: a review on sensitizers. *Anticancer Res.* **2014**, *34*, 4657−4664.
(12) Bonnet, S. Why develop photoactivated chemotherapy? *Dalton Trans.* **2018**, *47*, 10330−10343.
(13) Gong, Z.; Dai, Z. Design and Challenges of Sonodynamic Therapy System for Cancer Theranostics: From Equipment to Sensitizers. *Adv. Sci.* **2021**, *8*, 2002178.
(14) Imberti, C.; Zhang, P.; Huang, H.; Sadler, P. J. New designs for phototherapeutic transition metal complexes. *Angew. Chem. Int. Ed.* **2020**, *59*, 61−73.
(15) Mandal, A. A.; Kushwaha, R.; Yadav, A. K.; Banerjee, S. Metal Complexes for Cancer Sonodynamic Therapy. *ChemBioChem* **2023**, *24*, No. e202200597.
(16) Bonnet, S. Ruthenium-Based Photoactivated Chemotherapy. *J. Am. Chem. Soc.* **2023**, *145*, 23397−23415.
(17) Liang, C.; Xie, J.; Luo, S.; Huang, C.; Zhang, Q.; Huang, H.; Zhang, P. A highly potent ruthenium (II)-sonosensitizer and sonocatalyst for in vivo sonotherapy. *Nat. Commun.* **2021**, *12*, 5001.
(18) Banerjee, S.; Chakravarty, A. R. Metal Complexes of Curcumin for Cellular Imaging, Targeting and Photo-induced Anticancer Activity. *Acc. Chem. Res.* **2015**, *48*, 2075−2083.
(19) Pellei, M.; Del Bello, F.; Porchia, M.; Santini, C. Zinc coordination complexes as anticancer agents. *Coord. Chem. Rev.* **2021**, *445*, 214088.
(20) Mari, C.; Pierroz, V.; Ferrari, S.; Gasser, G. Combination of Ru (II) complexes and light: new frontiers in cancer therapy. *Chem. Sci.* **2015**, *6*, 2660−2686.
(21) Liu, Z.; Sadler, P. J. Organoiridium Complexes: Anticancer Agents and Catalysts. *Acc. Chem. Res.* **2014**, *47*, 1174−1185.
(22) Deng, Z.; Zhu, G. Beyond mere DNA damage: Recent progress in platinum(IV) anticancer complexes containing multi-functional axial ligands. *Curr. Opin. Chem. Biol.* **2023**, *74*, 102303.
(23) Kushwaha, R.; Kumar, A.; Saha, S.; Bajpai, S.; Yadav, A. K.; Banerjee, S. Os(II) complexes for Catalytic Anticancer Therapy: Recent Update. *Chem. Commun.* **2022**, *58*, 4825−4836.
(24) Lai, Y.; Lu, N.; Ouyang, A.; Zhang, Q.; Zhang, P. Ferroptosis promotes sonodynamic therapy: a platinum (II)−indocyanine sonosensitizer. *Chem. Sci.* **2022**, *13*, 9921−9926.
(25) Leonidova, A.; Gasser, G. Underestimated Potential of Organometallic Rhenium Complexes as Anticancer Agents. *ACS Chem. Biol.* **2014**, *9*, 2180−2193.
(26) Marker, S. C.; MacMillan, S. N.; Zipfel, W. R.; Li, Z.; Ford, P. C.; Wilson, J. J. Photoactivated in Vitro Anticancer Activity of Rhenium(I) Tricarbonyl Complexes Bearing Water-Soluble Phosphines. *Inorg. Chem.* **2018**, *57*, 1311−1331.
(27) (a) Chakraborty, I.; Carrington, S. J.; Roseman, G.; Mascharak, P. K. Synthesis, Structures, and CO Release Capacity of a Family of WaterSoluble PhotoCORMs: Assessment of the Biocompatibility and Their Phototoxicity toward Human Breast Cancer Cells. *Inorg. Chem.* **2017**, *56*, 1534−1545. (b) Gonzales, M. A.; Mascharak, P. K. Photoactive metal carbonyl complexes as potential agents for targeted CO delivery. *J. Inorg. Biochem.* **2014**, *133*, 127−135. (c) Carrington, S. J.; Chakraborty, I.; Bernard, J. M.; Mascharak, P. K. Synthesis and Characterization of a "Turn-On" photoCORM for Trackable CO Delivery to Biological Targets. *ACS Med. Chem. Lett.* **2014**, *5*, 1324−1328.
(28) Pan, Z. Y.; Cai, D.-H.; He, L. Dinuclear phosphorescent rhenium(I) complexes as potential anticancer and photodynamic therapy agents. *Dalton Trans.* **2020**, *49*, 11583−11590.
(29) Feng, W.-W.; Liang, B.-F.; Chen, B.-H.; Liu, Q.-Y.; Pan, Z.-Y.; Liu, Y.-J.; He, L. A tricarbonyl rhenium(I) complex decorated with boron dipyrromethene for endoplasmic reticulum-targeted photodynamic therapy. *Dyes Pigm.* **2023**, *211*, 111077.
(30) Leonidova, A.; Pierroz, V.; Rubbiani, R.; Heier, J.; Ferrari, S.; Gasser, G. Towards cancer cell-specific phototoxic organometallic rhenium(I) complexes. *Dalton Trans.* **2014**, *43*, 4287−4294.
(31) Leonidova, A.; Pierroz, V.; Rubbiani, R.; Lan, Y.; Schmitz, A. G.; Kaech, A.; Sigel, R. K. O.; Ferrari, S.; Gasser, G. Photo-induced uncaging of a specific Re(I) organometallic complex in living cells. *Chem. Sci.* **2014**, *5*, 4044−4056.
(32) Maisuls, I.; Cabrerizo, F. M.; David-Gara, P. M.; Epe, B.; Ruiz, G. T. DNA oxidation photoinduced by norharmane rhenium(I) polypyridyl complexes: Effect of the bidentate N,N'-ligands on the damage profile. *Chem.—Eur. J.* **2018**, *24*, 12902−12911.
(33) (a) Kastl, A.; Dieckmann, S.; Wähler, K.; Völker, T.; Kastl, L.; Merkel, A. L.; Vultur, A.; Shannan, B.; Harms, K.; Ocker, M.; Parak,

https://doi.org/10.1021/acs.jmedchem.3c02485
J. Med. Chem. 2024, 67, 6537−6548

W. J.; Herlyn, M.; Meggers, E. Rhenium complexes with visible-light-induced anticancer activity. *ChemMedChem* **2013**, *8*, 924−927. (b) Wähler, K.; Ludewig, A.; Szabo, P.; Harms, K.; Meggers, E. Rhenium Complexes with Red-Light-Induced Anticancer Activity. *Eur. J. Inorg. Chem.* **2014**, *2014*, 807−811.

(34) Mion, G.; Gianferrara, T.; Bergamo, A.; Gasser, G.; Pierroz, V.; Rubbiani, R.; Vilar, R.; Leczkowska, A.; Alessio, E. Phototoxic activity and DNA interactions of water-soluble porphyrins and their rhenium(I) conjugates. *ChemMedChem* **2015**, *10*, 1901−1914.

(35) (a) Li, C.; Pang, Y.; Xu, Y.; Lu, M.; Tu, L.; Li, Q.; Sharma, A.; Guo, Z.; Li, X.; Sun, Y. Near-Infrared Metal Agents Assisting Precision Medicine: From Strategic Design to Bioimaging and Therapeutic Applications. *Chem. Soc. Rev.* **2023**, *52*, 4392−4442. (b) Costa, D. F.; Mendes, L. P.; Torchilin, V. P. The effect of low- and high-penetration light on localized cancer therapy. *Adv. Drug Delivery Rev.* **2019**, *138*, 105−116. (c) Wan, G. Y.; Wan, G. Y.; Liu, Y.; Chen, B. W.; Liu, Y. Y.; Wang, Y. S.; Zhang, N.; Liu, Y.; Chen, B. W.; Liu, Y. Y.; et al. Recent advances of sonodynamic therapy in cancer treatment. *Cancer Biol. Med.* **2016**, *13*, 325−338.

(36) Zhu, J.; Ouyang, A.; He, J.; Xie, J.; Banerjee, S.; Zhang, Q.; Zhang, P. An ultrasound-activated cyanine-rhenium (I) complex for sonodynamic and gas synergistic therapy. *Chem. Commun.* **2022**, *58*, 3314−3317.

(37) (a) Hieber, W.; Fuchs, H. Über Metallcarbonyle. XXXIX. Aminsubstituierte Rheniumcarbonyle. *Z. Anorg. Allg. Chem.* **1941**, *248*, 269−275. (b) Hieber, W. Metal Carbonyls, Forty Years of Research. *Adv. Organomet. Chem.* **1970**, *8*, 1−28.

(38) Chakraborty, I.; Jimenez, J.; Sameera, W. M. C.; Kato, M.; Mascharak, P. K. Luminescent Re(I) Carbonyl Complexes as Trackable PhotoCORMs for CO delivery to Cellular Targets. *Inorg. Chem.* **2017**, *56*, 2863−2873.

(39) Świtlicka-Olszewska, A.; Klemens, T.; Nawrot, I.; Machura, B.; Kruszynski, R. Novel Re(I) tricarbonyl coordination compound of 5-amino-1,10-phenanthroline - Synthesis, structural, photophysical and computational studies. *J. Lumin.* **2016**, *171*, 166−175.

(40) Carreño, A.; Solís-Céspedes, E.; Zúñiga, C.; Nevermann, J.; Rivera-Zaldívar, M. M.; Gacitúa, M.; Ramírez-Osorio, A.; Páez-Hernández, D.; Arratia-Pérez, R.; Fuentes, J. A. Cyclic voltammetry, relativistic DFT calculations and biological test of cytotoxicity in walled-cell models of two classical rhenium (I) tricarbonyl complexes with 5-amine-1,10-phenanthroline. *Chem. Phys. Lett.* **2019**, *715*, 231−238.

(41) Kurtz, D. A.; Dhakal, B.; Hulme, R.; Nichol, G. S.; Felton, G. A. Correlations between photophysical and electrochemical properties for a series of new Mn carbonyl complexes containing substituted phenanthroline ligands. *Inorg. Chim. Acta* **2015**, *427*, 22−26.

(42) Busby, M.; Gabrielsson, A.; Matousek, P.; Towrie, M.; Di Bilio, A. J.; Gray, H. B.; Vlček, A. Excited-state dynamics of fac-$[ReI(L)(CO)_3(phen)]^+$ and fac-$[ReI(L)(CO)_3(5\text{-}NO_2\text{-}phen)]^+$ (L = imidazole, 4-ethylpyridine; phen = 1,10-phenanthroline) complexes. *Inorg. Chem.* **2004**, *43*, 4994−5002.

(43) Enslin, L. E.; Purkait, K.; Pozza, M. D.; Saubamea, B.; Mesdom, P.; Visser, H. G.; Gasser, G.; Schutte-Smith, M. Rhenium(I) Tricarbonyl Complexes of 1,10-Phenanthroline Derivatives with Unexpectedly High Cytotoxicity. *Inorg. Chem.* **2023**, *62*, 12237−12251.

(44) Frisch, M. J.; Trucks, G. W.; Schlegel, H. B.; Scuseria, G. E.; Robb; Cheeseman, J. R.; Scalmani, G.; Barone, S. V.; Petersson, G. A.; Nakatsuji, H.; Li, X.; et al. *Gaussian 16*. Revision A.03; Gaussian Inc.: Wallingford, CT, 2016.

(45) Kushwaha, R.; Singh, V.; Peters, S.; Yadav, A. K.; Dolui, D.; Saha, S.; Sarkar, S.; Dutta, A.; Koch, B.; Sadhukhan, T.; Banerjee, S. Density Functional Theory-Guided Photo-Triggered Anticancer Activity of Curcumin-Based Zinc(II) Complexes. *J. Phys. Chem. B* **2023**, *127*, 10266−10278.

(46) Liang, G.; Sadhukhan, T.; Banerjee, S.; Tang, D.; Zhang, H.; Cui, M.; Montesdeoca, N.; Karges, J.; Xiao, H. Reduction of Platinum(IV) Prodrug Hemoglobin Nanoparticles with Deeply Penetrating Ultrasound Radiation for Tumor-Targeted Therapeutically Enhanced Anticancer Therapy. *Angew. Chem., Int. Ed.* **2023**, *62*, No. e202301074.

(47) Puckett, C. A.; Barton, J. K. Methods to Explore Cellular Uptake of Ruthenium Complexes. *J. Am. Chem. Soc.* **2007**, *129*, 46−47.

(48) Konkankit, C. C.; Marker, S. C.; Knopf, K. M.; Wilson, J. J. Anticancer activity of complexes of the third-row transition metals, rhenium, osmium, and iridium. *Dalton Trans.* **2018**, *47*, 9934−9974.

(49) Karges, J. Clinical development of metal complexes as photosensitizers for photodynamic therapy of cancer. *Angew. Chem., Int. Ed.* **2022**, *61*, No. e202112236.

(50) Bera, A.; Gautam, S.; Sahoo, S.; Pal, A. K.; Kondaiah, P.; Chakravarty, A. R. Red light active Pt(IV)-BODIPY prodrug as a mitochondria and endoplasmic reticulum targeted chemo-PDT agent. *RSC Med. Chem.* **2022**, *13*, 1526−1539.

(51) Su, X.; Wang, W.; Cao, Q.; Zhang, H.; Liu, B.; Ling, Y.; Zhou, X.; Mao, Z. A Carbonic Anhydrase IX (CAIX)-Anchored Rhenium(I) Photosensitizer Evokes Pyroptosis for Enhanced Anti-Tumor Immunity. *Angew. Chem., Int. Ed.* **2022**, *61*, No. e202115800.

(52) (a) Knopf, K. M.; Murphy, B. L.; MacMillan, S. N.; Baskin, J. M.; Barr, M. P.; Boros, E.; Wilson, J. J. In Vitro Anticancer Activity and in Vivo Biodistribution of Rhenium(I) Tricarbonyl Aqua Complexes. *J. Am. Chem. Soc.* **2017**, *139*, 14302−14314. (b) Neuditschko, B.; King, A. P.; Huang, Z.; Janker, L.; Bileck, A.; Borutzki, Y.; Marker, S. C.; Gerner, C.; Wilson, J. J.; Meier-Menches, S. M. An Anticancer Rhenium Tricarbonyl Targets Fe-S Cluster Biogenesis in Ovarian Cancer Cells. *Angew. Chem. Int. Ed.* **2022**, *61*, No. e202209136.

(53) van Meerloo, J.; Kaspers, G. J.; Cloos, J. Cell sensitivity assays: the MTT assay. *Methods Mol. Biol.* **2011**, *731*, 237−245.

(54) Das, U.; Shanavas, S.; Nagendra, A. H.; Kar, B.; Roy, N.; Vardhan, S.; Sahoo, S. K.; Panda, D.; Bose, B.; Paira, P. Luminescent 11-{Naphthalen-1-yl}dipyrido[3,2-a:2′,3′-c]phenazine-Based Ru(II)/Ir(III)/Re(I) Complexes for HCT-116 Colorectal Cancer Stem Cell Therapy. *ACS Appl. Bio Mater.* **2023**, *6*, 410−424.

(55) Kuznetcova, I.; Bacher, F.; Alfadul, S. M.; Tham, M. J. R.; Ang, W. H.; Babak, M. V.; Rapta, P.; Arion, V. B. Elucidation of Structure-Activity Relationships in Indolobenzazepine-Derived Ligands and Their Copper(II) Complexes: The Role of Key Structural Components and Insight into the Mechanism of Action. *Inorg. Chem.* **2022**, *61*, 10167−10181.

(56) He, L.; Pan, Z. Y.; Qin, W. W.; Li, Y.; Tan, C. P.; Mao, Z. W. Impairment of the autophagy-related lysosomal degradation pathway by an anticancer rhenium(I) complex. *Dalton Trans.* **2019**, *48*, 4398−4404.

(57) Mani, A.; Feng, T.; Gandioso, A.; Vinck, R.; Notaro, A.; Gourdon, L.; Burckel, P.; Saubaméa, B.; Blacque, O.; Cariou, K.; Belgaied, J.-E.; Chao, H.; Gasser, G. Structurally Simple Osmium(II) Polypyridyl Complexes as Photosensitizers for Photodynamic Therapy in the Near Infrared. *Angew. Chem. Int. Ed.* **2023**, *62*, No. e202218347.

(58) Zhang, P.; Wang, Y.; Qiu, K.; Zhao, Z.; Hu, R.; He, C.; Zhang, Q.; Chao, H. A NIR phosphorescent osmium(II) complex as a lysosome tracking reagent and photodynamic therapeutic agent. *Chem. Commun.* **2017**, *53*, 12341−12344.

(59) Li, Y.; Lu, N.; Lin, Q.; Wang, H.; Liang, Z.; Lu, Y.; Zhang, P. Sono-ReCORMs for synergetic sonodynamic-gas therapy of hypoxic tumor. *Chin. Chem. Lett.* **2023**, *34*, 107653.

(60) Cao, X.; Li, M.; Liu, Q.; Zhao, J.; Lu, X.; Wang, J. Inorganic Sonosensitizers for Sonodynamic Therapy in Cancer Treatment. *Small* **2023**, *19*, No. e2303195.

(61) Singh, V.; Rana, N. K.; Kashif, M.; Manna, P. P.; Basu Baul, T. S.; Koch, B. Aqua-(2-formylbenzoato)triphenyltin(IV) induces cell cycle arrest and apoptosis in hypoxic triple negative breast cancer cells. *Toxicol. in Vitro* **2023**, *86*, 105484.

(62) (a) Son, S.; Kim, J. H.; Wang, X.; Zhang, C.; Yoon, S. A.; Shin, J.; Sharma, A.; Lee, M. H.; Cheng, L.; Wu, J.; Kim, J. S. Multifunctional sonosensitizers in sonodynamic cancer therapy. *Chem. Soc. Rev.* **2020**, *49*, 3244−3261. (b) Liang, S.; Deng, X.; Ma,

https://doi.org/10.1021/acs.jmedchem.3c02485
J. Med. Chem. 2024, 67, 6537−6548

P.; Cheng, Z.; Lin, J. Recent Advances in Nanomaterial-Assisted Combinational Sonodynamic Cancer Therapy. *Adv. Mater.* **2020**, *32*, No. e2003214.
(63) (a) Zhu, P.; Chen, Y.; Shi, J. Nanoenzyme-Augmented Cancer Sonodynamic Therapy by Catalytic Tumor Oxygenation. *ACS Nano* **2018**, *12*, 3780−3795. (b) Hou, L.; Gong, F.; Han, Z.; Wang, Y.; Yang, Y.; Cheng, S.; Yang, N.; Liu, Z.; Cheng, L. $H_XV_2O_5$ Nanocatalysts Combined with Ultrasound for Triple Amplification of Oxidative Stress to Enhance Cancer Catalytic Therapy. *Angew. Chem. Int. Ed.* **2022**, *61*, No. e202208849. (c) Karanlık, C. C.; Atmaca, G. Y.; Erdoğmuş, A. Comparison of singlet oxygen production of ethyl vanillin substituted silicon phthalocyanine using sonophotodynamic and photodynamic methods. *J. Mol. Struct.* **2023**, *1274*, 134498. (d) Xu, Y.; Pang, Y.; Luo, L.; Sharma, A.; Yang, J.; Li, C.; Liu, S.; Zhan, J.; Sun, Y. De Novo Designed Ru(II) Metallacycle as a Microenvironment-Adaptive Sonosensitizer and Sonocatalyst for Multidrug-Resistant Biofilms Eradication. *Angew. Chem. Int. Ed.* **2024**, *63*, No. e202319966.
(64) Heinemann, F. W.; Karges, J.; Gasser, G. Critical Overview of the Use of Ru(II) Polypyridyl Complexes as Photosensitizers in One-Photon and Two-Photon Photodynamic Therapy. *Acc. Chem. Res.* **2017**, *50*, 2727−2736.
(65) Wasserman, H. H.; Scheffer, J.; Cooper, J. L. Singlet oxygen reactions with 9, 10-diphenylanthracene peroxide. *J. Am. Chem. Soc.* **1972**, *94*, 4991−4996.
(66) Huang, H.; Banerjee, S.; Qiu, K.; Zhang, P.; Blacque, O.; Malcomson, T.; Paterson, M. J.; Clarkson, G. J.; Staniforth, M.; Stavros, V. G.; Gasser, G.; Chao, H.; Sadler, P. J. Targeted photoredox catalysis in cancer cells. *Nat. Chem.* **2019**, *11*, 1041−1048.
(67) Huang, C.; Liang, C.; Sadhukhan, T.; Banerjee, S.; Fan, Z.; Li, T.; Zhu, Z.; Zhang, P.; Raghavachari, K.; Huang, H. In-vitro and In-vivo Photocatalytic Cancer Therapy with Bio-compatible Iridium(III) Photocatalysts. *Angew. Chem. Int. Ed.* **2021**, *60*, 9474−9479.
(68) Fan, Z.; Xie, J.; Sadhukhan, T.; Liang, C.; Huang, C.; Li, W.; Li, T.; Zhang, P.; Banerjee, S.; Raghavachari, K.; Huang, H. Highly Efficient Ir(III)-Coumarin Photo-Redox Catalyst for Synergetic Multi-Mode Cancer Photo-Therapy. *Chem.—Eur. J.* **2022**, *28*, No. e202103346.
(69) Wei, L.; Kushwaha, R.; Dao, A.; Fan, Z.; Banerjee, S.; Huang, H. Axisymmetric bis-tridentate Ir(III) photoredox catalysts for anticancer phototherapy under hypoxia. *Chem. Commun.* **2023**, *59*, 3083−3086.
(70) Zhu, Z.; Wei, L.; Lai, Y.; Carter, O. W. L.; Banerjee, S.; Sadler, P. J.; Huang, H. Photocatalytic glucose-appended bio-compatible Ir(III) anticancer complexes. *Dalton Trans.* **2022**, *51*, 10875−10879.
(71) Fan, Z.; Rong, Y.; Sadhukhan, T.; Liang, S.; Li, W.; Yuan, Z.; Zhu, Z.; Guo, S.; Ji, S.; Wang, J.; Kushwaha, R.; Banerjee, S.; Raghavachari, K.; Huang, H. Single-Cell Quantification of a Highly Biocompatible Dinuclear Iridium(III) Complex for Photocatalytic Cancer Therapy. *Angew. Chem. Int. Ed.* **2022**, *61*, No. e202202098.
(72) Wei, S.; Liang, H.; Dao, A.; Xie, Y.; Cao, F.; Ren, Q.; Yadav, A. K.; Kushwaha, R.; Mandal, A. A.; Banerjee, S.; Zhang, P.; Ji, S.; Huang, H. Perturbing tumor cell metabolism with a Ru(II) photoredox catalyst to reverse the multidrug resistance of lung cancer. *Sci. China Chem.* **2023**, *66*, 1482−1488.
(73) Fan, Z.; Xie, J.; Kushwaha, R.; Liang, S.; Li, W.; Mandal, A. A.; Wei, L.; Banerjee, S.; Huang, H. Anticancer Screening of Ru(II) Photoredox Catalysts at Single Cancer Cell Level. *Chem.—Asian J.* **2023**, *18*, No. e202300047.
(74) (a) Vaidya, S. P.; Patra, M. Platinum glycoconjugates: "Sweet bullets" for targeted cancer therapy. *Curr. Opin. Chem. Biol.* **2023**, *72*, 102236. (b) Patra, M.; Gasser, G. Organometallic compounds: an opportunity for chemical biology? *ChemBioChem* **2012**, *13*, 1232−1252.
(75) Sharma, G.; Rana, N. K.; Singh, P.; Dubey, P.; Pandey, D. S.; Koch, B. p53 dependent apoptosis and cell cycle delay induced by heteroleptic complexes in human cervical cancer cells. *Biomed. Pharmacother.* **2017**, *88*, 218−231.

https://doi.org/10.1021/acs.jmedchem.3c02485
J. Med. Chem. 2024, 67, 6537−6548